EUB/AGS Special Report 88

Deep Electrical Structure of the Buffalo Head Hills, Northern Alberta: Implications for Diamond Exploration

Alberta Energy and Utilities Board
Alberta Geological Survey

EUB/AGS Special Report 88

Deep Electrical Structure of the Buffalo Head Hills, Northern Alberta: Implications for Diamond Exploration

Erşan Türkoğlu[1], Martyn Unsworth[1] and Dinu Pana[2]

[1] University of Alberta
[2] Alberta Energy and Utilities Board/Alberta Geological Survey

May 2007

ISBN 0-7785-3847-8

This product is an EUB/AGS Special Report, the information is provided as received from the author and has had limited editing for conformity to EUB/AGS standards.

E. Türkoğlu, M. J. Unsworth and D. Pana, (2007): Deep electrical structure of Buffalo Head Hills, Northern Alberta; Implications for diamond exploration; Alberta Energy and Utilities Board, EUB/AGS Special Report 88, 34 p.

Author addresses:

Department of Physics
Room #238 CEB
11322 - 89 Avenue
University of Alberta
Edmonton Alberta CANADA
T6G 2G7
Phone: (780) 492-5286
Fax: (780) 492-0714

Published May 2007 by:

Alberta Energy and Utilities Board
Alberta Geological Survey
4th Floor, Twin Atria Building
4999 – 98th Avenue
Edmonton, Alberta
T6B 2X3
Canada

Tel: (780) 422-1927
Fax: (780) 422-1918
E-mail: EUB.AGS-Infosales@gov.ab.ca
Website: www.ags.gov.ab.ca

Contents

Figures

Acknowledgments

The authors are grateful to Wolfgang Soyer, Andrea Cochrane and Eylem Türkoğlu for assistance with magnetotelluric data collection. Roger Paulen of the Alberta Geological Survey is thanked for identifying surface materials along the transect and at each measurement site. Funding for this research was provided by the Alberta Ingenuity Fund, NSERC, the Canadian Foundation for Innovation, ISRIP and the Alberta Geological Survey. The 3-D magnetotelluric (MT) inversions used the algorithm supplied by Weerachai Siripunvaraporn, and the 2-D MT inversions were made possible by the algorithm supplied by Randy Mackie. Computation was made possible by the use of WestGrid computing resources. Maps were prepared using Generic Mapping Tools of Paul Wessel and Walter H. F. Smith.

Abstract

Geophysical studies in the Northwest Territories have shown that diamondiferous kimberlite pipes are spatially coincident with a zone of high electrical conductivity in the upper mantle. It has been suggested that the elevated conductivity is due to graphite, which may indicate a carbon-rich mantle, with carbon present as diamonds at greater depth. Magnetotelluric studies of the Trans-Hudson orogen detected a lithospheric mantle conductor close to the Fort à la Corne kimberlite field, which has similar geometrical and electrical properties to that in the Slave craton. The apparent spatial coincidence between diamondiferous kimberlites and an underlying mantle with peculiar geophysical properties may be a useful tool in area selection for diamond exploration. To test this hypothesis, the University of Alberta and the Alberta Geological Survey undertook long period magnetotelluric (MT) data collection across the Buffalo Head Hills kimberlite field of north-central Alberta, a region where a significant quantity of similar MT data had been previously acquired in the LITHOPROBE program.

MT data have been recorded at 13 locations spaced at approximately 24 km along Highway 88 between Lesser Lake Slave and the town of Vermilion, using University of Alberta instrumentation. Apparent resistivity and phase, as a function of signal period, were computed from the time series. Tensor decomposition showed a preferred geoelectric strike direction of N37°E, which, as expected, is roughly parallel to the geometry of the basement terranes. Two-dimensional (2-D) MT inversion was used to convert signal period into depth for both the new MT data and the previously reported LITHOPROBE data. Resulting resistivity models of the Earth showed a decrease in electrical resistivity at a depth of approximately 200 km that is interpreted as the lithosphere-asthenosphere boundary (LAB). A low resistivity (high conductivity) zone was observed in the upper mantle at 50 to 80 km depth beneath the northern end of the Buffalo Head Hills. Three-dimensional (3-D) inversions produced similar resistivity models to those obtained by 2-D inversions of individual profiles.

Similar upper mantle conductors have been reported beneath kimberlite fields in Northwest Territories and Saskatchewan. In each case, the low resistivity has been explained with elevated concentrations of graphite, although it must be noted that the low resistivity in the upper mantle can also be accounted for by the presence of partial melting and sulphide minerals. In contrast to the Slave craton, the northern Alberta upper mantle conductor is not directly below the kimberlites. This may indicate that a simple spatial correlation of diamondiferous kimberlite and upper mantle resistivity anomalies are not universal. Additional MT data are required to better constrain a 3-D resistivity model of northern Alberta and validate the 2-D approach used in this study.

1 Introduction

Diamonds are formed in lithospheric roots where pressures are high enough for carbon to be found as diamond rather than graphite (Boyd and Gurney, 1986). Diamond formation also requires that these roots are cold enough for the necessary high pressures to occur in the lithosphere rather than the asthenosphere. Most diamonds have been found in Archean lithosphere, and only occasionally in Proterozoic lithosphere as, for example, in northern Australia (Clifford, 1966). Diamonds are brought to the surface as inclusions in kimberlitic magmas, and, thus, diamond exploration is focused on the search for kimberlite pipes. Even with exploration limited to regions of thick, Archean lithosphere, the search for kimberlite pipes that contain diamonds requires very large areas to be covered. Additional criteria for area selection are invaluable for effective diamond exploration.

Magnetotelluric (MT) studies have recently been used to study the electrical resistivity structure of the lithosphere in the Northwest Territories (Jones and Craven, 2004). This study showed that the diamondiferous kimberlite pipes in the Slave craton are spatially associated with an anomalously low electrical resistivity (high conductivity) in the upper mantle. Several compositional factors, such as graphite, brines, partial melt and sulphides, can produce a low resistivity in the upper mantle. Jones and Craven (2004) excluded partial melting in the upper mantle (as inconsistent with existing seismic data) and sulphides (because they were not found in mantle xenoliths), and suggested that the low electrical resistivity beneath the Slave craton was due to the presence of interconnected graphite films. They speculated that the presence of graphite in the upper mantle could imply that, at greater depths in the diamond stability field, a carbon-rich mantle would contain diamonds. The electrical resistivity of carbon varies by eight orders of magnitude according to the structure. It has a resistivity of 10^{-4} to 10^{-10} Ωm when in graphite form and around 10^{12} Ωm when in diamond form.

In addition to locating carbon at upper mantle depths, deep electrical resistivity studies with MT can give other relevant information for diamond exploration. MT data can directly determine the thickness of the lithosphere by identifying the lithosphere-asthenosphere boundary (LAB), which is associated with a decrease in electrical resistivity. The lithospheric mantle typically has a resistivity 100–10,000 Ωm (Xu et al., 2000) and two factors cause a decrease in electrical resistivity with increasing temperature. The first occurs below the melting point as thermal activation allows electrons and ions to move more easily through the mineral lattice. The second factor occurs as partial melting begins and permits ions to easily move through the melt and allow electric current to flow. Most crustal and upper mantle rocks form partial melts with the melt well interconnected at low melt fractions owing to a low dihedral (wetting) angle. Laboratory experiments by Schilling et al., (1997) and Partzsch et al., (2000) showed that 2% partial melting occurs in typical mantle rocks at 1030°C and that the resistivity of the molten rock at melt fractions above 3% is almost independent of the resistivity of the solid phase (Partzsch et al., 2000). Thus, an increase of temperature from 1030°C to 1100°C can produce a factor of ten decreases in resistivity that can be readily detected with a long-period magnetotelluric survey (Figure 1).

If the spatial correlation of diamondiferous kimberlites and upper mantle conductors is true, this has profound implications for diamond exploration. In this report we describe MT data collected in the Buffalo Head Hills of Northern Alberta in an attempt to test the working hypothesis of a direct spatial correlation between upper mantle conductors and diamondiferous kimberlite pipes.

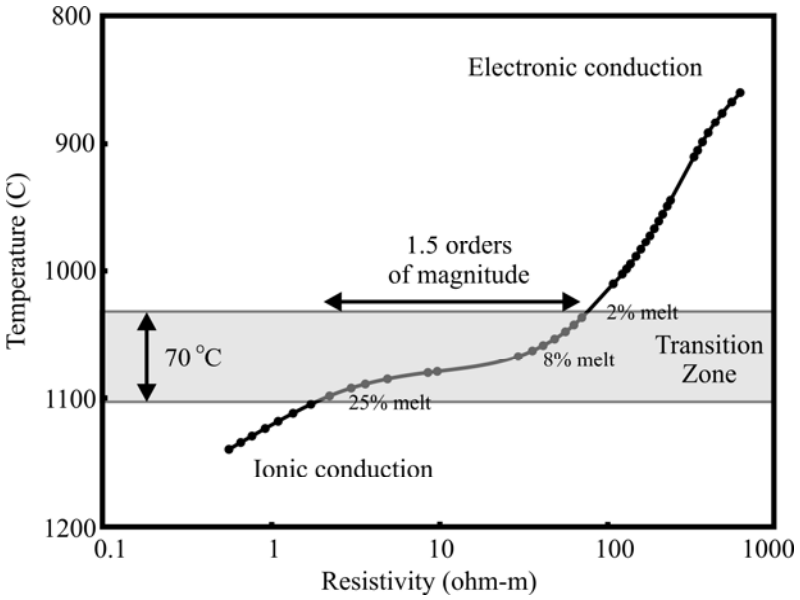

Figure 1. Resistivity-temperature experiment of Partzsch et al., (2000). A melt fraction of at least 8% is required to have interconnectivity. The transition from electronic to ionic conduction occurs within 70°C (redrawn from Jones and Craven, 2004).

2 Geological Setting

Surface geology in the field area is characterized by glacial deposits of varying thickness, which overly 1-2 km of Phanerozoic strata of the Western Canada Sedimentary Basin (WCSB) overlying Precambrian crystalline basement rocks. A brief review of these units from top to bottom follows.

The present physiography of the area is the result of multiple glaciations. Glacial advances in northern Alberta originated from the Laurentide Ice Sheet, which generally flowed across central Alberta in a southwesterly direction (Fulton, 1989). Unconsolidated drift thickness varies from less than 2 m in the Buffalo Head Hills to more than 200 m in the Loon River Lowlands, particularly within the following major paleovalleys: (1) the Wabasca–Loon River paleovalley that roughly coincides with the Loon River lowlands; (2) the northwest-trending Muskwa River paleovalley; and (3) the area east of Peerless Lake. In the Buffalo Head Hills, areas of thin (< 2 m) till overlie bedrock shale and sandstone of the Smoky Group and Wapiti Formation (Hamilton et al., 1999; Pawlowicz et al., 2005a,b; Paulen et al., 2006). A thin veneer of preglacial quartzite gravels, likely Tertiary, locally overlies the bedrock at the highest elevations of shallow drift cover (Trommelen, 2004; Paulen et al., 2006). At surface, glacial sediments dominate which include till, glaciolacustrine clay and glaciofluvial outwash, and post glacial sediments such as, organic deposits, alluvium, colluvium and eolian sediments, all in relative order of abundance (Paulen et al., 2006). Satellite imagery analysis of the Buffalo Head Hills-Loon River area led to the identification of a large number of lineaments with four general orientations that were interpreted to mark bedrock faults (Paganelli et al., 2003).

Phanerozoic strata form a southwest thickening wedge ranging from 1200 to 2000 metres thick in the study area and increasing to about 6000 m in front of the Cordilleran fold-and-thrust belt. A sub-Cretaceous unconformity divides the Phanerozoic cover into two successions deposited in two fundamentally different tectonosedimentary environments: (a) a Middle Devonian to Lower Mississippian succession deposited in a passive continental margin and (b) an upper Early to lower Late Cretaceous foreland basin succession (Price, 1994; Ross and Eaton, 1999). Middle Devonian formations progressively onlap southwest onto the east-northeast trending Late Proterozoic to Late Devonian basement uplift known as the Peace River Arch (PRA). During the Paleozoic, the Buffalo Head Hills-

Loon River area was a shallow shelf to basinal marine setting dominated by carbonate, shale and evaporite deposits. The uppermost Devonian and Mississippian strata thicken southwestwardly as the PRA collapsed and were eroded in the uplifted northeast. During Cretaceous time, the investigated area became part of the Cordilleran foreland basin and Paleozoic formations were unconformably blanketed by the Lower Cretaceous marine shales with wedges of sand and silt deposits (Chen and Olson, 2005). Upper Cretaceous formations consist of a sequence of alternating marine and nonmarine Cretaceous sandstone and shale, incised and eroded down to the Shaftesbury Formation in the Loon River lowland. The bedrock has limited exposure along the northern and eastern flanks of the Buffalo Head Hills and is largely covered southeast of the Buffalo Head Hills by unconsolidated glacial deposits of variable thickness. Although several kimberlite diatremes crop out or form topographic highs up to 60 m above the surrounding terrain, most are covered by variable thicknesses (up to 127 m) of fine- to coarse-grained glaciolacustrine and glaciofluvial sediments.

The Buffalo Head Hills kimberlite field consists of pyroclastic-crater facies lapilli-bearing olivine crystal tuff that is stratigraphically dominated by normally graded beds of coarse ash to coarse crystal tuff and juvenile lapilli-rich beds (Carlson et al., 1998; Skelton et al., 2003; Eccles, 2004). At least 26 of the 38 occurrences of kimberlite are reported to be diamondiferous and five with higher microdiamond counts (K252, K5, K6, K11, K14, and K91) have been sampled by Ashton Mining of Canada Inc. since1998 (e.g., Ashton Mining of Canada Inc. Press Release 1998; 1999; 2001). Xenoliths are typically Late Cretaceous shale with rare crystalline basement and mantle xenoliths. The peridotite suite includes spinel lherzolite, garnet-spinel-lherzolite, calcic garnet harzburgites and sheared garnet lherzolite (Carlson et al., 1998; Skelton et al., 2003). Xenocryst mineral compositions of kimberlites in the central Buffalo Head Hills region indicate the mantle is characterized by lherzolitic, wehrlitic and websteritic garnet compositions (Hood and McCandless, 2004). Mantle xenolith and diamond inclusion studies suggest the underlying basement is Early Proterozoic, primarily lherzolitic in composition, and that the LAB is at about 180 km depth (Aulbach et al., 2004; Davies et al., 2004). Zircon U-Pb laser ablation ages from a quartz diorite xenolith recovered from the K6 kimberlite indicate the basement has been affected by a tectonothermal event around 1940 Ma (Eccles et al., 2006) similar to the Taltson magmatic zone to the east.

The Precambrian basement of north-central Alberta is represented by Archean crust variably reworked during the Early Proterozoic, which has been assigned to distinct continental slivers accreted to the Rae Terrane during the Hudsonian tectonism (~2.0 to 1.8 Ga; Ross et al., 1994) or to the westernmost portion of the Rae Terrane (Burwash et al., 2000; Chacko et al., 2000; De et al., 2000). In the investigated area, the crystalline basement is part of the Buffalo Head domain, a 200 to 300 km wide, elongate region of internally complex, north-trending, westward convex, moderately positive aeromagnetic anomalies with negative septa (e.g., Ross et al., 1994; Pilkington et al., 2000). It may be divisible into three subdomains: to the west, the "Buffalo Head high;" to the east, the "Utikuma Belt;" and to the south, a broad negative anomaly with little internal fabric (Ross et al., 1991). Drillcore samples recovered from the Buffalo Head domain are mainly metaplutonic rocks ranging in composition from gabbro to leucogranite, with minor metavolcanic and high-grade gneissic rocks (Thériault and Ross, 1991; Burwash et al., 2000). The centre of Buffalo Head domain, including the area under investigation, consists of the Red Earth granulite domain (Burwash at al., 2002). Mineral assemblages of garnet-potassium-feldspar±cordierite±sillimanite and the common occurrence of orthopyroxene indicate high-grade (granulite-facies) metamorphic conditions. Within the Red Earth granulite domain lies an elliptical negative gravity anomaly, possibly reflecting the presence of a granite pluton (Trout Mountain Pluton of Burwash et al., 2000) or a zone of deformation.

U-Pb crystallization ages obtained from core are in the range 2324 to 1993 Ma, with four occurrences of plutonic rocks in the narrow age range 1999 to 1993 Ma (Villeneuve et al., 1993). Initial εNd values scatter over the +0.2 to –6.3 range, whereas T_{DM} model ages vary from 2.83 to 2.51 Ga, with a preponderance of 2.8 to 2.7 Ga ages and are in the same range as the adjacent Taltson magmatic zone to the east (Thériault, 1992). Recent U-Th-Pb monazite chemical ages from core samples from the Peerless

Lake map sheet (NTS 84B) range from 2020 Ma in gneiss and granite to ca. 1900 Ma in blastomylonite and retrogressed granulite (Rangers, 2004), which indicates a similar tectonothermal history of the Buffalo Head domain as the Taltson magmatic zone and western Churchill Province. Geochemical and isotopic compositions of granitic rocks from the Taltson magmatic zone indicate an intracrustal origin, in a plate interior setting (Chacko et al., 2000).

The area under investigation is situated immediately east of the PRA. Long lasting structural disturbance within the PRA, greatly affected the Phanerozoic stratigraphy in northwestern Alberta (Cant, 1988; O'Connell et al., 1990) and extended in the Cretaceous time in the Buffalo Head Hills-Loon River study area and possibly across most of northern Alberta (Pană et al., 2001). Although fault offsets in the Phanerozoic stratigraphy are bellow the resolution of log interpretation-based stratigraphic studies, several lineaments trending north, northeast, northwest and east have been inferred based on a swarm of basement highs and lows interpreted to show preferred orientations and some spatial coincidences with oil and gas pools in the overlying strata (Chen and Olson, 2005). The conventional wisdom is that such faults in the basement may have been formed or reactivated during the Late Cretaceous to create pathways for kimberlite magma into the Late Cretaceous strata.

3 Previous Geophysical Studies in Northern Alberta

This area of Northern Alberta is well known for its wealth of hydrocarbon resources. With the exception of well-log data, the results of most detailed geological and geophysical investigations, including high resolution aeromagnetic (HRAM) and seismic reflection data remain in the private domain. Publicly available stratigraphic and structural data in the area are limited. In early 1995, the Alberta Energy Company conducted a fixed-wing aeromagnetic survey in the region to assist in the interpretation of the Precambrian basement terranes for oil and gas exploration. Ten shallow high-frequency magnetic anomalies corresponding to strong diffractions and unusual reflections on existing seismic profiles turned out to be kimberlite pipes. Diamond exploration conducted in the following years by Ashton Mining of Canada Inc. confirmed 37 kimberlite pipes in at least four spatially separate clusters (Ashton Mining of Canada Inc., 2002). Robertson (2003) studied the lightning strike database of northern Alberta and inferred a number of lineaments of higher density/intensity of lightning strikes along vaguely defined lineaments interpreted as possibly mineralized faults. Lyatsky and Pana (2003) processed regional gravity data for northern Alberta and identified a series of linear gravity anomalies that may represent basement faults.

Extensive magnetotelluric (MT) data collection took place as part of the LITHOPROBE Alberta Basement Transect (Boerner et al., 2000). This project collected long period MT data at 323 sites to study the Paleoproterozoic tectonics of the basement rocks. Dimensionality analysis of these data showed mainly 1-D structures for the basin and 2-D structures for the crustal depths, controlled by vertical and horizontal conductivity changes along the basement rocks of Alberta. Geoelectrical strike directions were found to be N35-45°E, which are roughly parallel to the internal grain and of magnetic domains for most of the stations for periods (penetration depths) corresponding to crustal depths. The Kiskatinaw conductor (KC) discovered in this survey follows the Kiskatinaw low-magnetic anomaly in northwest Alberta and northeastern British Columbia. The Red Deer conductor (RDC) in southcentral Alberta was well imaged and is approximately coincident with a magnetic anomaly along the Snowbird Tectonic Zone (STZ). Both of these crustal conductors are associated with inferred ancient suture zones (e.g., Ross et al., 1994) and the high conductivity (low resistivity) is believed to be a consequence of graphite concentration. A third crustal conductivity anomaly was identified from the reversal of the induction vectors southwest of Lesser Slave Lake. These conductors were identified from transverse electric (TE) mode data that is derived from electric currents flowing parallel to these structures. Conductors can also be identified by a reversal in direction of induction vectors (see below for details). These thin crustal conductors are essentially invisible in the transverse magnetic (TM) data. Boerner et al. (1999) also studied the long-period (deep

sounding) MT data across the Archean Churchill Province (ACP) and the Snowbird Tectonic Zone. Two-dimensional conductivity models showed that the upper mantle beneath the Archean Terranes was more conductive than the upper mantle beneath the Paleoproterozoic crustal rocks by one order of magnitude. This observation was interpreted as tectonically induced metasomatism which had enhanced the electrical conductivity in the lithosphere.

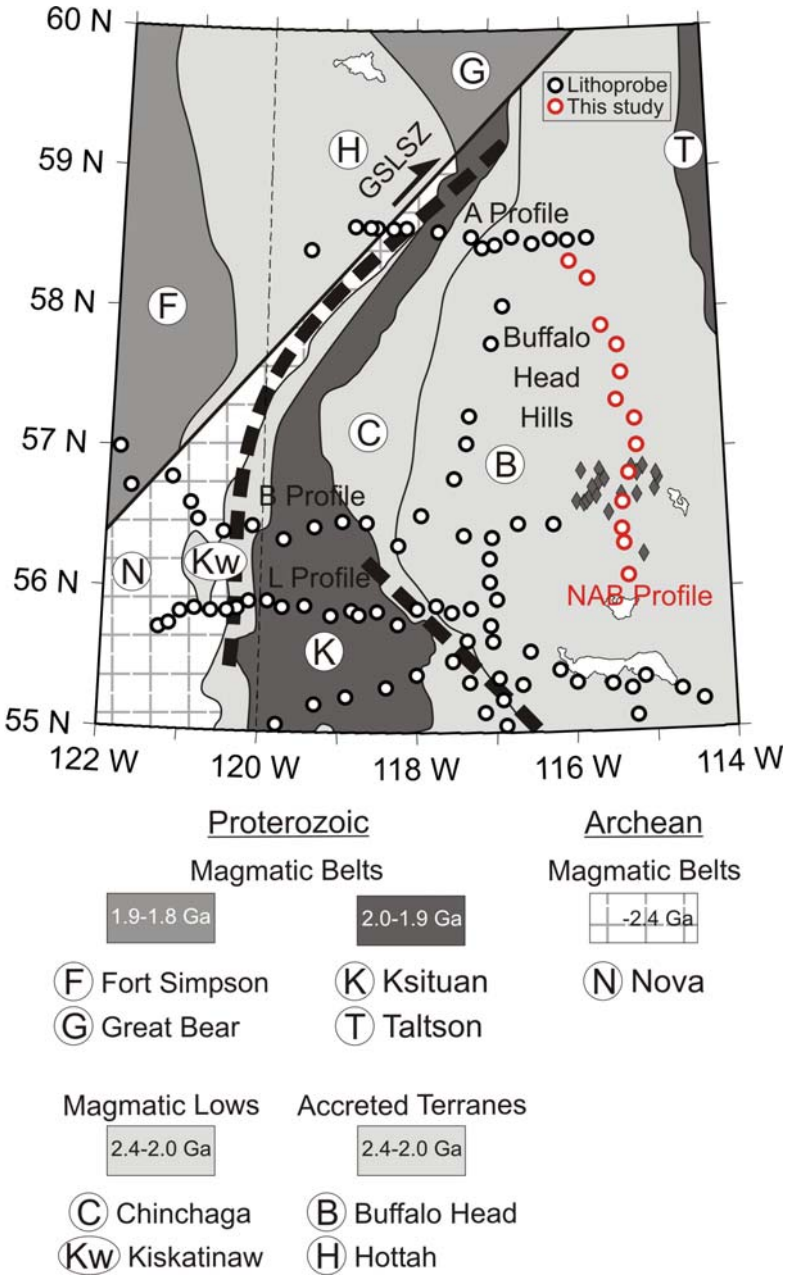

Figure 2. Basement geology of the study area derived from Villeneuve et al., (1993) based on potential field signatures, core samples and extrapolation of outcrop in the Canadian Shield. Diamonds show the kimberlitic pipes, small circles show the MT stations and dashed lines indicate the major conductivity anomalies in the study area (Boerner et al., 2000).

Teleseismic studies were used in south-central Alberta to determine the thickness of crust and lithosphere (Shragge et al., 2002). An inversion of P-wave travel times showed high seismic velocities beneath much of the southern Hearne Province extending to depths of 200 to 250 km, which was interpreted as the lithosphere-asthenosphere boundary. Therefore, high velocities beneath Archean crust suggest that the Hearne lithosphere remained intact with the assumption that previously reported conductivity anomaly from MT observations was caused by small volumes of connected hydrous or metallic minerals introduced during subduction. Shear wave-splitting showed a polarization aligned to a general N37-53°E trend, which is parallel to geologic and geoelectrical strike directions. Receiver function analysis of P-waves revealed a Moho depth of ~38 km in southern and central Alberta. This result is consistent with the LITHOPROBE active seismic data collected around Peace River where enhanced reflections imply an east-dipping Kiskatinaw-Ksituan boundary along lines 11 and 12 of the Peace River Arch Industry Seismic Experiment (PRAISE) data. The dip of the strong reflections was found to be ~25°E with the reflections disappearing at a depth of ~40 km (Ross and Eaton, 2002).

4 Magnetotelluric Data Collection

Long-period magnetotelluric (MT) data were collected in northern Alberta in May and June of 2004 at 13 locations. The profile extended from Utikuma Lake to Fort Vermilion, with an inter-station spacing of approximately 20 km (Figure 2). At each measurement location, MT data were recorded for one month using the NIMS long period magnetotelluric systems owned by the University of Alberta. In MT fieldwork, two orthogonal electric field and three magnetic field components are recorded as a function of time. These MT instruments use fluxgate magnetometers to measure the variations of the Earth's magnetic field with time. Electric fields were measured with non-polarizing electrodes buried 30 to 40 cm below the surface to avoid the effects of daily temperature variations and precipitation. To maintain a stable electrical contact with the ground, bentonite was placed into the electrode holes. The timing of each instrument was synchronized using signals from GPS satellites. The stations were deployed along Highway 88 where the only cultural noise was due to oil and gas pumps and pipelines. MT stations were placed at least 500 m away from pipelines to minimize the effects of noise arising from cathodic protection. The electric and magnetic field data were recorded at a rate of eight samples per second (Figure 3). Approximately 300 MB of time series data were recorded at each site.

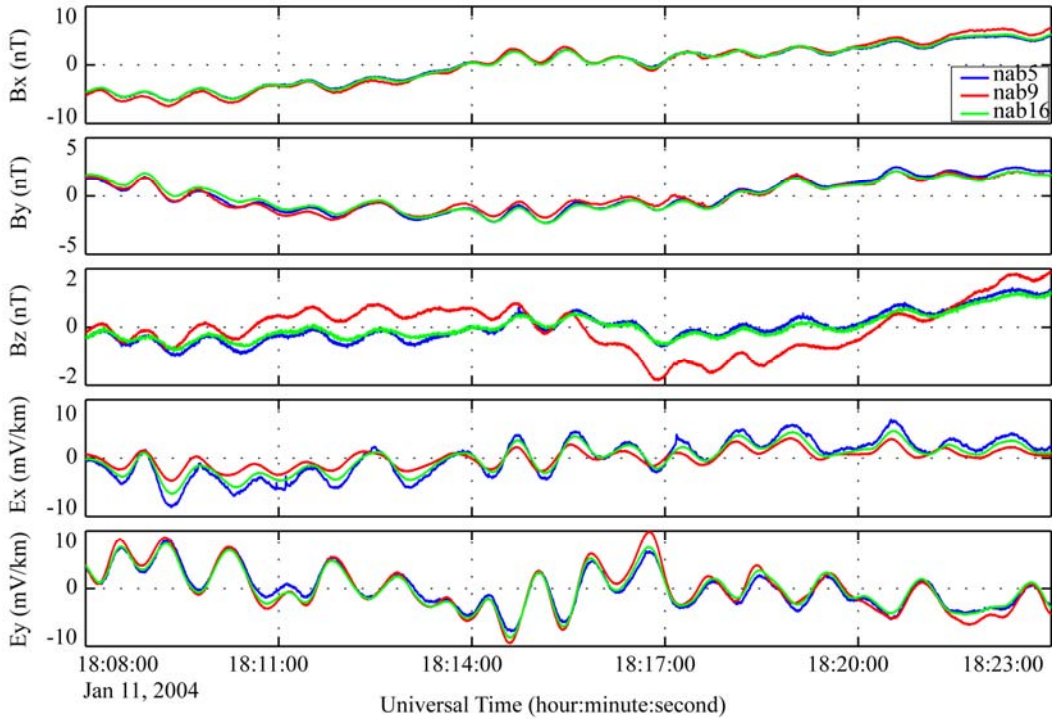

Figure 3. Simultaneous electric and magnetic fields recorded at three different sites. The repeating sinusoidal signals are Pc3 magnetic pulsations which originate in the interaction of the solar wind and the Earth's magnetosphere.

5 Magnetotelluric Data Analysis

The magnetotelluric method uses natural electromagnetic (EM) signals that penetrate into the earth. These electromagnetic (EM) fields are generated by worldwide lightning activity and by interactions between the solar wind and the magnetosphere over the period band 0.001–10000 seconds. Note that the period (T) of a signal, and the frequency (f) are related as $T = 1/f$. It can be shown that the depth of signal penetration is proportional to the period (T) of the signal as

$$\delta = 503\sqrt{\rho\, T} \quad \text{(m)} \qquad (1)$$

where ρ is the electrical resistivity of the Earth and the distance δ is called the skin depth. The MT method was independently discovered by Tikhonov (1950) and Cagniard (1953). Over the last twenty years, the method has become more widely used due to improved instrumentation and data analysis techniques (Unsworth, 2005). A detailed overview of MT data analysis is described by Vozoff (1991) and Simpson and Bahr (2005).

5.1 Time Series Analysis

The initial step of MT data analysis is to convert the measurements from the time domain to the frequency domain. The magnetotelluric method is based on the assumption that the electromagnetic signals – incident on the surface of the Earth – have a planar geometry. This assumption allows the electric and magnetic fields at the surface of the Earth to be related as

$$\mathbf{e}(T) = \mathbf{Z}(T)\mathbf{h}(T) + \varepsilon \qquad (2)$$

where, $\mathbf{e}(T)$ and $\mathbf{h}(T)$ are the electric and magnetic fields measured at a period T. The quantity $\mathbf{Z}(T)$ is the impedance of the ground and ε is the noise.
It can be shown that

$$\hat{\mathbf{Z}}(T) = \left\langle \mathbf{e}(T)\mathbf{h}(T)^* \right\rangle \left\langle \mathbf{h}(T)\mathbf{h}(T)^* \right\rangle^{-1}$$

where the brackets denote average of different time segments for a particular period or nearby frequencies and the superscript asterisk shows the conjugate transpose. The electrical resistivity can be extracted from the impedance as

$$\rho(T) = \frac{T}{2\pi\mu}\left|\mathbf{Z}(T)\right|^2 \qquad (3)$$

Since the depth of penetration varies with T, this provides an elegant way to determine the variation of resistivity with depth. An example of how apparent resistivity at station *nab5* varies with signal period (T) is shown in Figure 4. The apparent resistivity generally shows a smooth variation with period, as expected for high quality MT data. Note that some points at short period are scattered because of magnetic noise. This scatter can be removed by using a simultaneous magnetic field that contains the same MT signal but different noise (Gamble et al., 1979). The improvement achieved with this so-called remote reference technique is illustrated in Figure 4. Note that over the range 1 to 100 s the apparent resistivity increases corresponding to an increase in resistivity from the sedimentary cover of the WCSB to crystalline basement rocks. At periods longer than 300 s, the apparent resistivity decreases indicating that a conductor is present at depth.

5.2 Dimensionality of the Magnetotelluric Data

Two dimensional (2-D) interpretations of MT data are widely used and are computationally much simpler than a full three dimensional (3-D) analysis. However, implementation of a 2-D approach requires that the dimensionality and geoelectric strike direction is carefully evaluated.

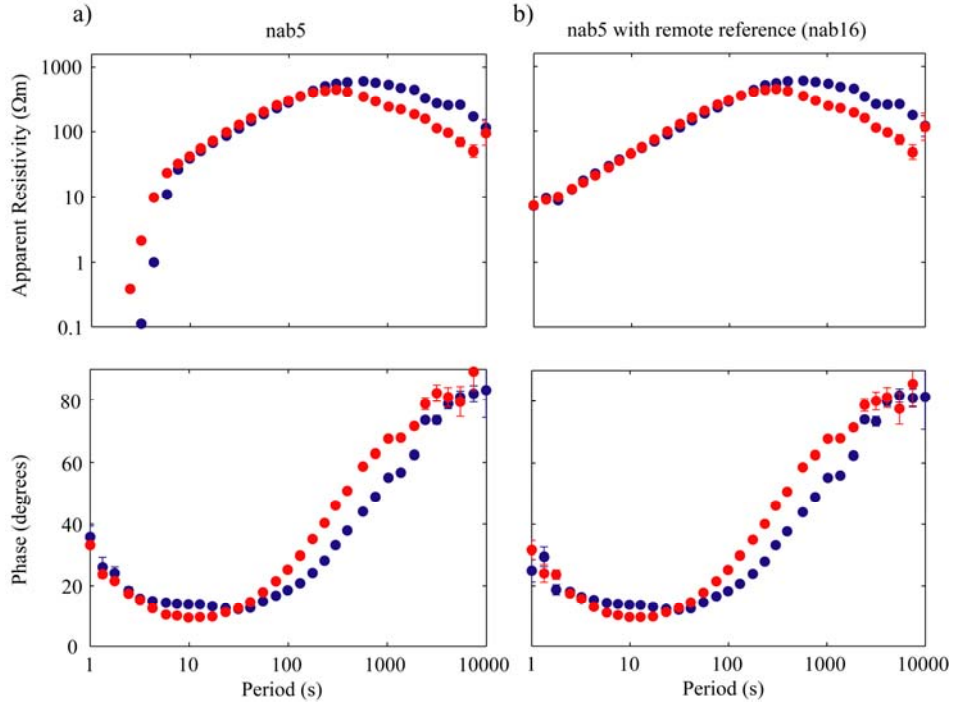

Figure 4. Apparent resistivity and phase curves for station nab5 in N37°E strike coordinate system. (a) Local processing of the data shows a severe downward bias for periods less than 10 seconds. (b) Use of magnetic field data recorded at another MT station (remote reference) improves the quality of the data through remote reference processing.

5.2.1 Skew and Strike

One widely used way of identifying the dimensionality of the impedance tensor is to plot the skew of the data (Swift, 1967 and Bahr, 1988). A skew value below 0.3 indicates that the structure is essentially 1-D or 2-D (Bahr, 1988). Skew values in excess of 0.3 are an indicator of 3-D resistivity structures.

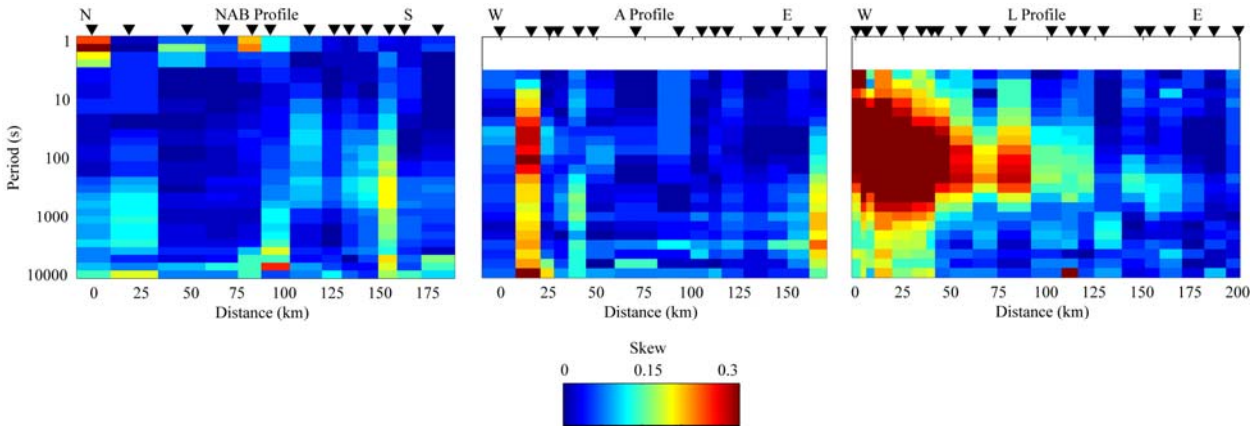

Figure 5. Skew values for NAB, A and L profiles for each period. NAB profile is north-south from left to right and other profiles are west-east from left to right. A skew value of greater than 0.3 generally indicates 3-D geoelectric structure.

Figure 5 shows the skew for the NAB profile and two of the LITHOPROBE profiles A and L in Northern Alberta (Figure 2). Note that in each figure distance along the profile is plotted on the horizontal axis, while period is plotted on the vertical axis. Since depth of penetration increases with period, this type of pseudo-section display gives an impression of depth on the vertical scale. The NAB profile and A profile appear to be quite 2-D, while the west end of the L profile show strong indications of 3-D effects at periods 10 to 1000 s. Dimensionality analysis of the LITHOPROBE MT stations using the approach of Weaver et al., (2000) showed that the eastern half of profile A can be considered 2-D while the stations analyzing the western half indicate 3-D effects for intermediate periods (Jones et al., 2002).

The geoelectric strike directions for the Northern Alberta data were then computed with the tensor decomposition algorithm of McNeice and Jones (2001) and are shown in Figures 6 and 7. Different period ranges were investigated to find the appropriate strike direction for the area and depth of interest. Note that the calculated MT strike has a fundamental 90° uncertainty, so the absolute strike cannot be determined using the MT data alone. Other information, such as knowledge of the local geology, is needed to overcome this ambiguity. To demonstrate the consistency of the strike along the profile, average strike values were plotted on maps (Figure 6) and rose diagrams (Figure 7) for various period bands.

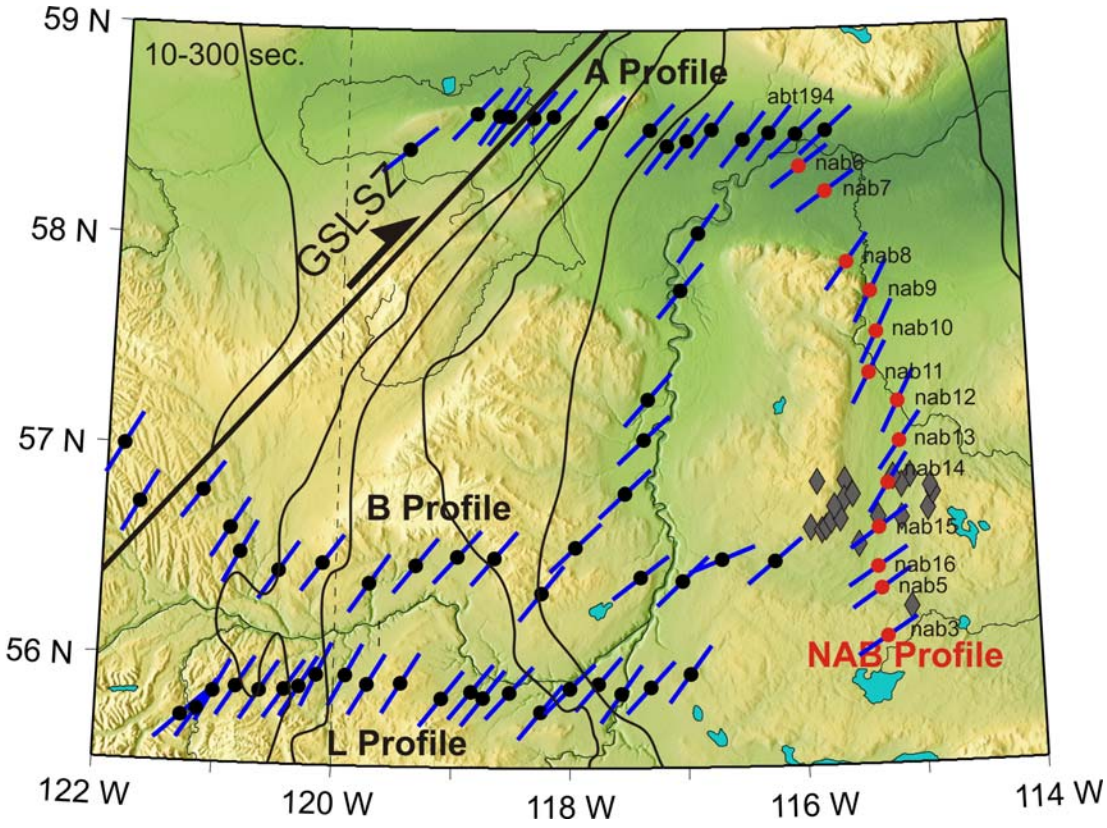

Figure 6. Geoelectric strike of the study area for periods of 10 to 300 seconds. Signals with these periods sample down to mid-crustal depths. Black dots represent LITHOPROBE MT data and red dots represent NAB data collected in this study. Solid lines indicate basement domains of Ross et al., 1994. Kimberlite pipes are denoted by diamond symbols

The average geoelectric strike of the region was found to be N35–40°E. The strike directions for the LITHOPROBE data show less site-to-site variation along the profiles compared to NAB profile. There is a 5–10^{o} change in the calculated strike for the stations from Red Earth Creek to the northern end of the Buffalo Head Hills, perhaps implying a geoelectric boundary almost parallel to NAB profile direction. This is likely due to variable thickness of the sedimentary cover in this area. A rose diagram was plotted for different period ranges. For the short periods (0–5 km penetration) the strike values are poorly determined, indicating an essentially 1-D geoelectric structure. Intermediate periods penetrate into the mid-crust and exhibit a well-defined strike for most sites in the range N35–45°E. These strike directions are consistent between the NAB and Profile A of Boerner et al., (2000). Boerner et al., (2000) calculated the strike for A profile to be N37°E. This angle is also an appropriate angle for the NAB profile.

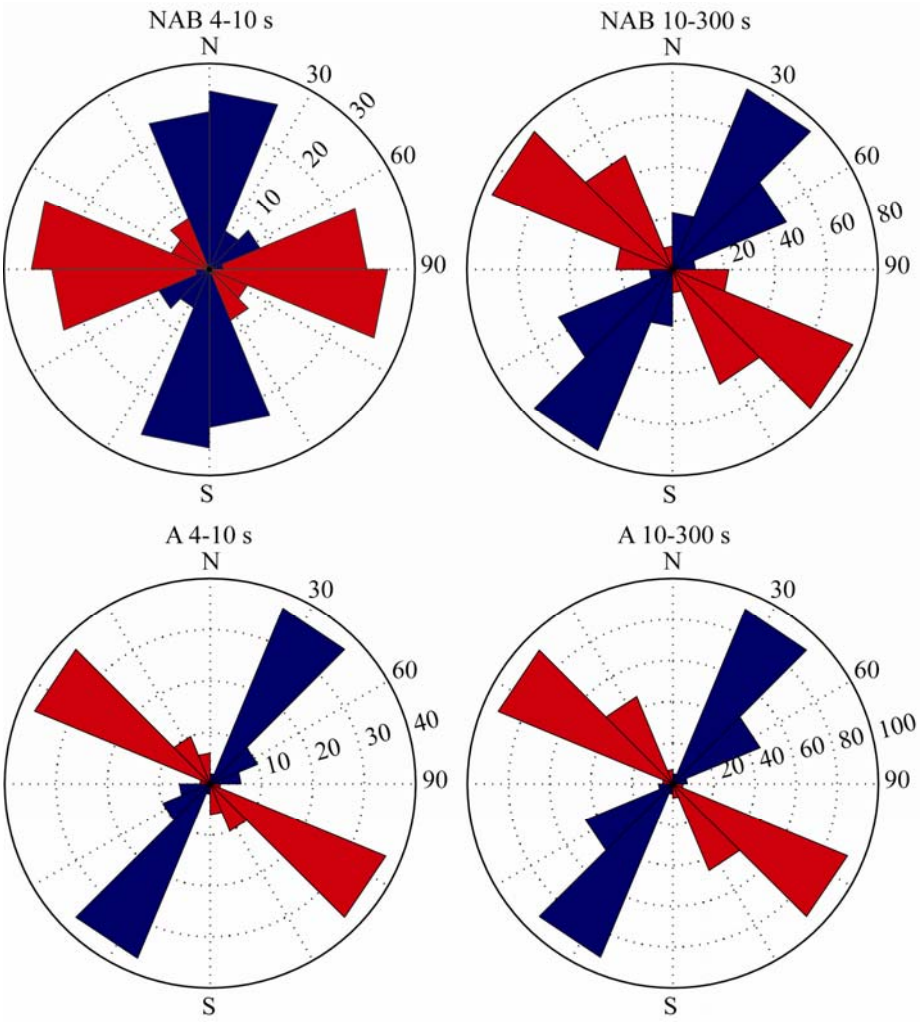

Figure 7. Rose diagrams for short (left) and intermediate periods (right) of the NAB (top) data compared to profile A of Boerner et al. (2000) (bottom). Inner circles show the number of occurrence. Blue and red sections represent the 90° uncertainty in MT strike direction.

5.2.2 Induction Vectors

The ratio of vertical to horizontal magnetic field variations at a MT station is often called the tipper (Vozoff, 1991). Tipper data ($\mathbf{T_x}$ and $\mathbf{T_y}$) can be used to identify the enhanced current in the earth and can be expressed as a pair of real and imaginary induction arrows which have a magnitude (L) and an azimuth (φ). Since these values are not related to impedance, they provide independent constraints on the resistivity structure of the area.

$$\mathbf{H_z} = \mathbf{T_x}\,\mathbf{H_x} + \mathbf{T_y}\,\mathbf{H_y} \qquad (6)$$

$$\mathrm{L} = \sqrt{\left|\mathbf{T}_x\right|^2 + \left|\mathbf{T}_y\right|^2} \qquad (7)$$

$$\varphi = \arctan\left(\frac{\mathbf{T}_y}{\mathbf{T}_x}\right) \tag{8}$$

The real part of these vectors can be plotted on a map either pointing away from the conductor (Schmucker, 1970) or pointing towards the conductor (Parkinson, 1959). These vectors can provide valuable constraints on the dimensionality and strike analysis of the data as they are independent of the MT impedance tensor. In this report the Schmucker's notation is used in which the induction vectors point away from conductors. The behavior of these vectors can be complex when there are 3-D structures or anisotropy effects in the data (Heise and Pous, 2001). Two dimensional interpretations of these vectors help understanding the geometry and integrated inversion of this data with TE and TM modes improves the location and shape of the conductive anomalies considerably by providing additional information due to their sensitivity to lateral resistivity distributions. The induction vectors were plotted using Schmucker's notation for different periods as shown in Figure 8. Previous interpretations of the Lithoprobe MT data revealed two main low resistivity zones in the study area (Boerner et al., 2000). One is the Kiskatinaw conductor, which crosses A, B and L profiles with azimuths of 45 to 53° NE. The other conductor starts just south of Lesser Slave Lake and extends NW to the end of the L profile. In general, all of the induction vectors in this area are coherent and showing systematic variations for increasing depths.

For short periods (~30 s), the induction vectors are small, which implies a 1-D (layered) structure. For intermediate periods (~300 s), the length of the induction vectors increases and there is little variation in direction from station-to-station. The NAB data does not show any anomalous directions and angles, implying that a large conductor is not located below or close by this profile. Long period induction vectors show influence from different conductors. This is particularly the case with the slowly disappearing anomalous induction vectors, which point away from each other on the E profile for intermediate periods. Furthermore, the directions of the vectors rotate clockwise. This rotation is more pronounced on the eastern stations.

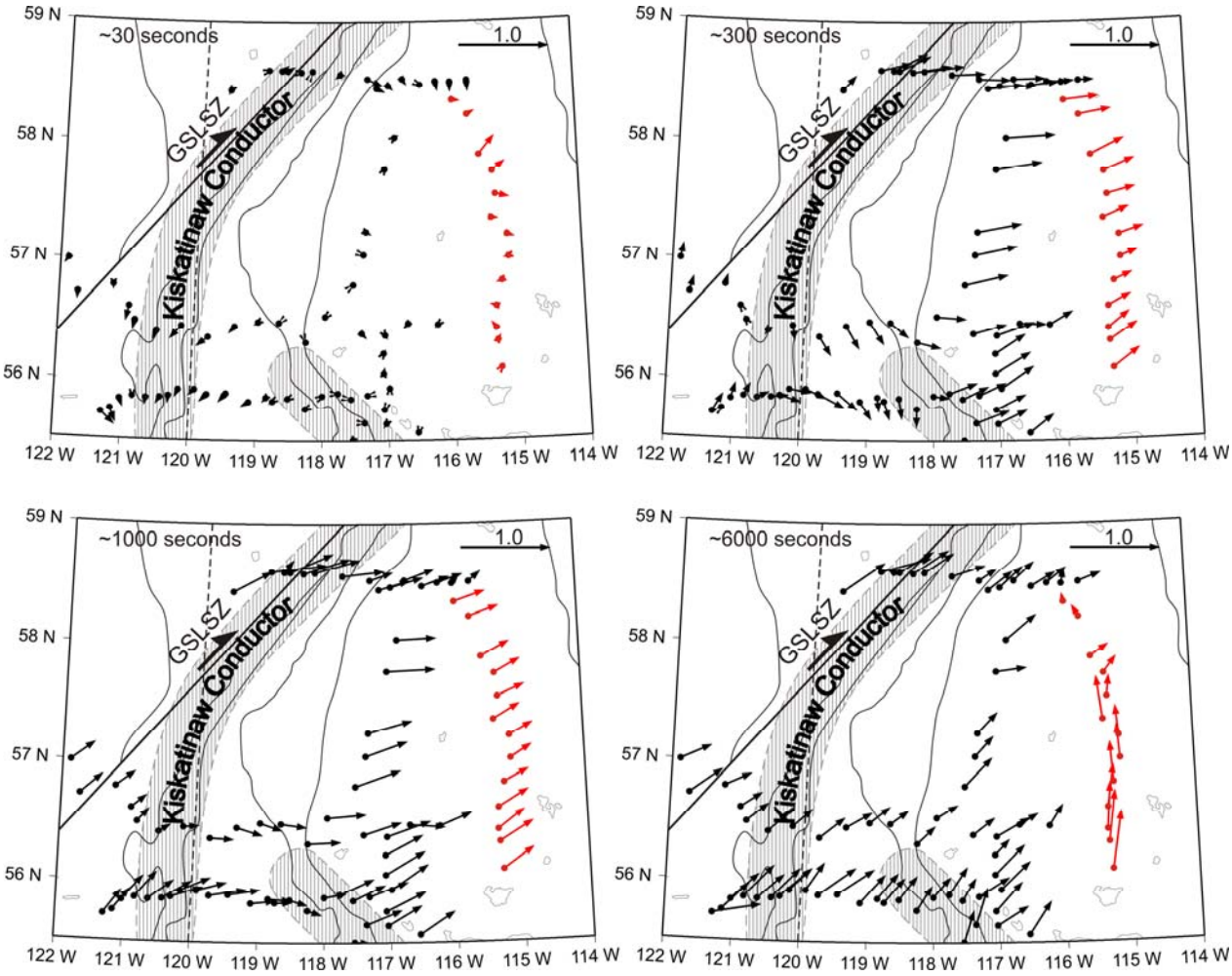

Figure 8. Real induction vectors for the NAB and LITHOPROBE MT data. Red dots show NAB sites.

5.3 Apparent Resistivity and Phase Curves

The data were rotated into a N37°E coordinate frame and apparent resistivity curves at 6 representative stations on the NAB profile are shown in Figure 9. Note that at each site two curves are shown. The curve called *TE* is computed from E_x and H_y, where *x* is parallel to the strike direction derived from tensor decomposition, and *y* is perpendicular to the strike. The *TM* curve is computed from E_y and H_x. If the Earth has a layered, one-dimensional structure then it can be shown that these curves will be coincident. If these two quantities are not equal, then the subsurface resistivity structure is 2-D or 3-D. In a 2-D scenario the electromagnetic fields can be divided into two groups. The transverse electric (TE) mode comprises the electric field parallel to the strike direction, while the transverse magnetic (TM) mode has a magnetic field parallel to the geoelectric strike. In the TE mode electric currents are parallel to the geoelectric strike direction, whereas in the TM mode the current flow is perpendicular the strike direction. Therefore, the two modes are sensitive to different aspects of subsurface structure. The TE mode is responsive to conductive anomalies while TM mode is more sensitive to resistive parts of the data and to the shallow sections of the subsurface. The joint inversion of these two modes significantly improves the results of MT interpretations. In this report both separate and joint inversion are presented to show the different aspects of the MT data.

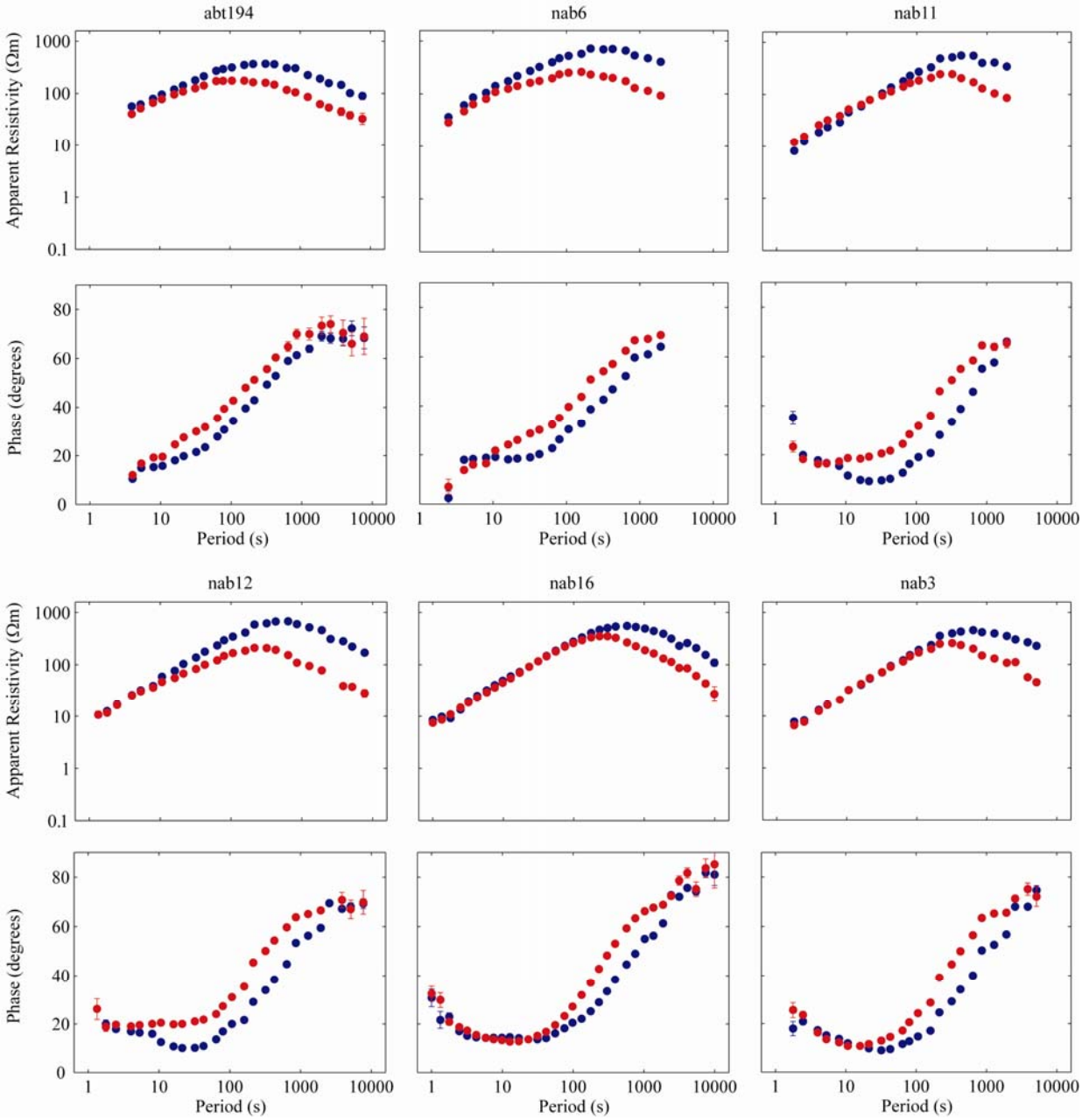

Figure 9. Apparent resistivity and phase curves along the profile starting from north (top left corner) to south (bottom right corner) in N37°E strike coordinate system; red dots - TE mode, blue dots – TM mode (see text). Only the data points used in the inversion are shown for representative stations.

From Figure 9, it can be seen that the TE and TM curves are quite similar, indicating the structure is relatively 1-D. The apparent resistivity increases over the period range 1 to 300 s implying an increase in resistivity with depth in the crust and lithosphere. At periods beyond 300 s the apparent resistivity decreases, implying a low resistivity layer at depth. This basic shape of the apparent resistivity curve is observed at all stations, except for the northern stations (nab6, nab7 and abt194). MT data can also be plotted in pseudosection format (Figure 10) depicting resistivity variations along the profile. Note that as period is plotted on the vertical axis this gives an impression of depth variations since larger periods penetrate to greater depths,

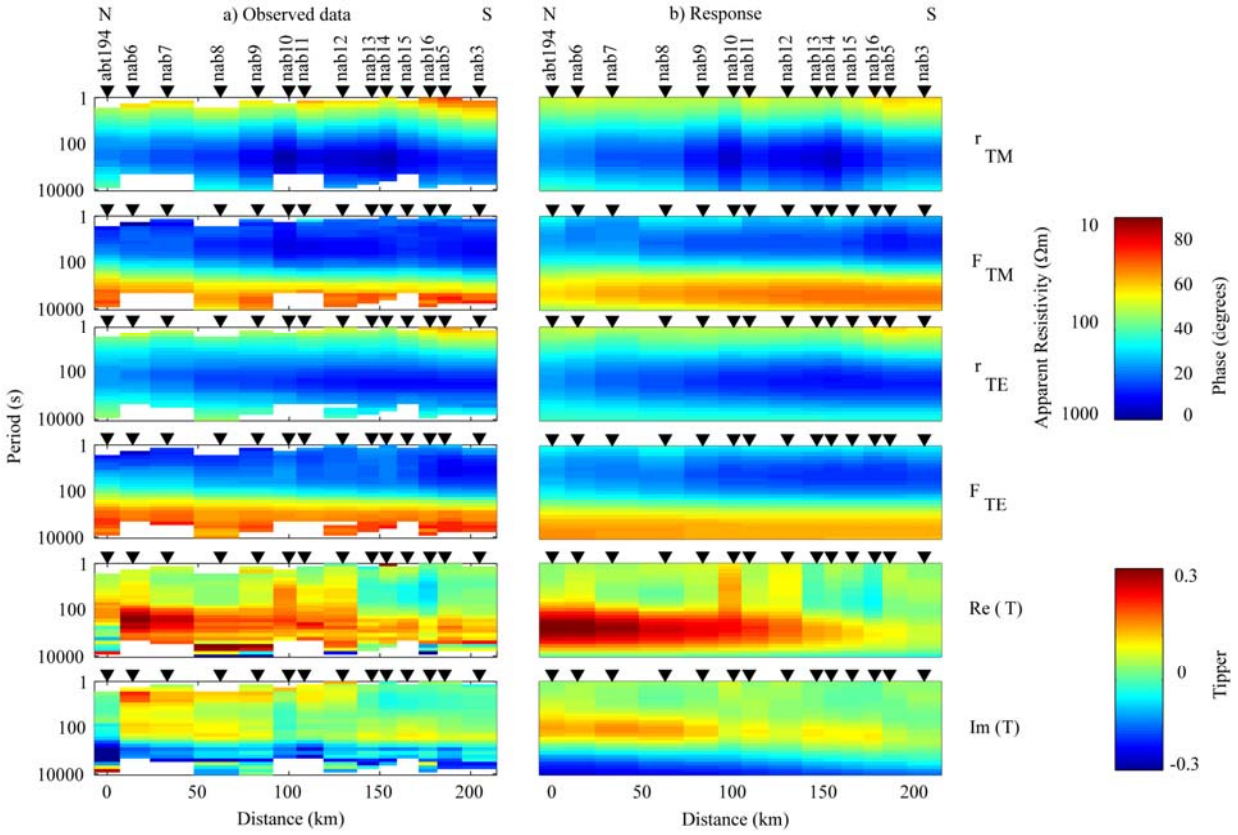

Figure 10. (a) Magnetotelluric impedance data and vertical magnetic field transfer functions (tipper) in pseudosection format for the NAB profile in N37°E coordinates. (b) Response of the 2-D inversion model in Figure 15b. White areas in the observed data pseudosection show noisy data that were excluded from the inversion.

6 Inversion of Magnetotelluric Data

Once the dimensionality of an MT dataset is understood, the apparent resistivity and phase data can be converted into a resistivity model with the appropriate dimensionality. This requires that the data is converted from being a function of frequency to being a function of depth. This can be achieved through trial and error forward modelling or, more commonly, through the use of automated inversion algorithms. Most inversion schemes start with a homogenous half-space model and repeatedly update the resistivity model until it fits the observed MT data to a specified degree. It can be shown that this process is non-unique, which means that many models can be found to fit the measured MT data. A common approach to overcome this problem is to impose the requirement that an acceptable resistivity model both fits the measured MT data and is also spatially smooth. If the resistivity structure in the study area is 2-D or 3-D then the application of 1-D MT inversion can give very misleading results.

6.1 Two-Dimensional Inversion of NAB Magnetotelluric Data

It was shown in section 5.2 that dimensionality criteria suggest that a 2-D inversion of the NAB is valid. The MT data were rotated to the geoelectric strike direction (N37°E) determined in section 5.2 and all the stations were projected onto a profile perpendicular to the strike direction. The MT data were then inverted using the 2-D inversion algorithm of Rodi and Mackie (2001). This algorithm uses several control parameters that allow the requirement of spatial smoothness to be systematically varied. One parameter is τ, which controls the trade-off between the degree of smoothing and fit to the measured MT data. The other parameter is α, which controls the vertical to horizontal smoothing of the model. Many

inversions were performed with the goal of finding a resistivity model that was not dependent on a specific choice of control parameters. Initial inversions have considered the TE and TM modes separately (Figure 11). The TM mode inversion shows a shallow layer (0–5 km) of low resistivity (~10 Ωm) that corresponds to the sedimentary basin in the region underlain by a very homogenous and resistive half-space on the southern half of the profile (Figure 11a). The TE inversion in Figure 11b also shows a shallow, low resistivity layer, that is underlain by high resistivities (5–100 km depth) and a low resistivity layer below a depth of 150 km. Both inversions yielded a good fit to the measured MT data. This is quantified by the root-mean-square (r.m.s) misfit, which should ideally be in the range 1–1.5. In this case, the r.m.s. misfit values were 1.1 for the TE mode and 1.5 for the TM mode.

A joint inversion of the TE and TM mode data is required to find the most comprehensive resistivity model of the subsurface. The vertical magnetic transfer functions (tipper) data were also included in the inversion. The final r.m.s. misfit of the joint TE-TM-tipper inversion was 1.4 and the resistivity model is shown in Figure 12a. The pseudosections in Figure 10 show that the final model response reproduces the observed data for TE, TM and tipper data adequately for all the stations and the whole period band.

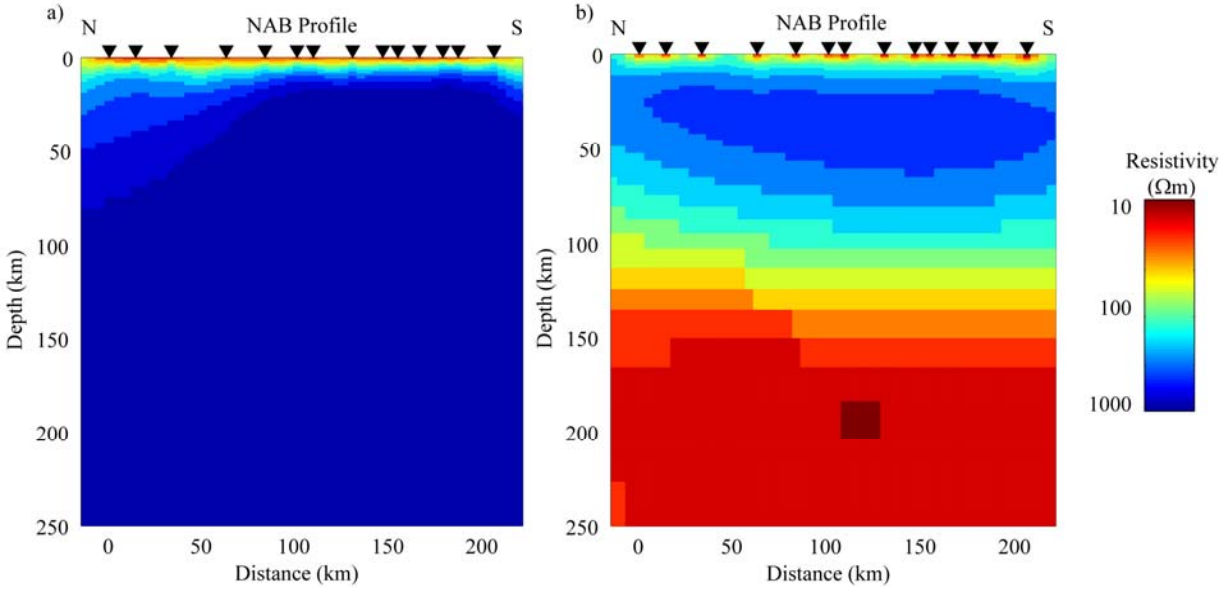

Figure 11. Individual mode inversions of the NAB data. (a) TM-mode and (b) TE-mode inversions. Error floor of 20% was applied to the apparent resistivity and error floor of 10% was applied to the phase data. Control parameters used were τ =10 and α =3.

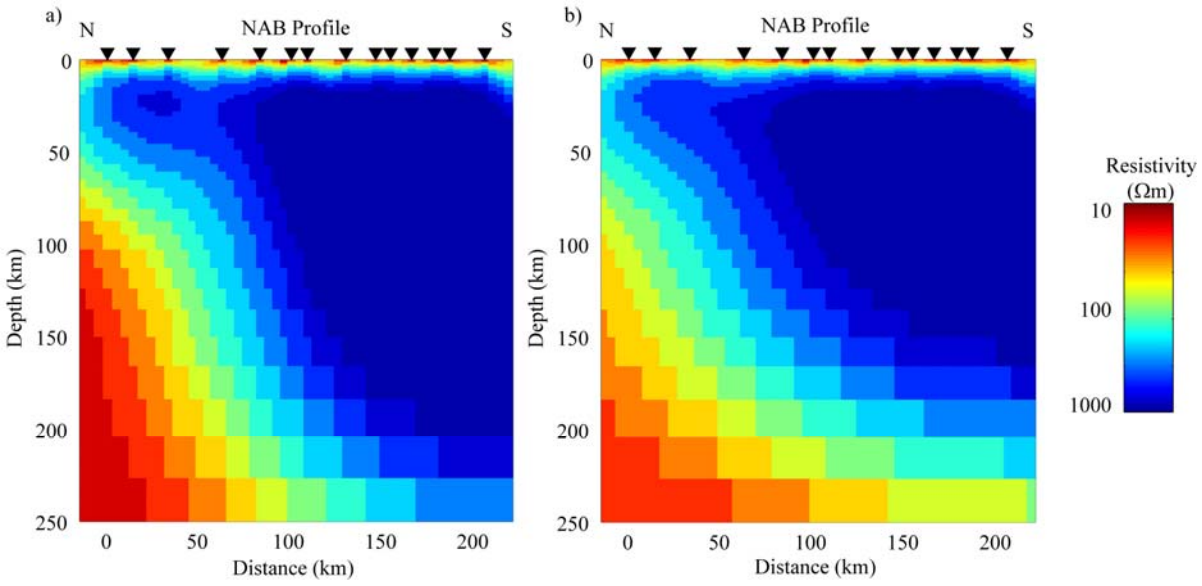

Figure 12. TE, TM and tipper joint inversion of the NAB profile. a) τ =10 and α =1, b) τ =10 and α =3. The northernmost station is abt194 from the LITHOPROBE MT data.

To verify the stability of the inversion and the presence of the conductor at the northern end, a number of different inversions were performed with different control parameters. Every inversion resulted in a strong conductor at the north end of the profile, although the shape varied (Figure 12). The inversion in Figure 12a used the default parameters τ =10 and α =1 and gave an r.m.s. misfit of 1.3 after 200 iterations. Figure 12b used τ =10 and α =3 and the r.m.s. of the final model is 1.4 after 200 iterations. To examine if the conductor shown in Figure 12 is regional in extent, the LITHOPROBE A-profile data were inverted using the same procedure. The A-profile and NAB models are shown together in Figure 13. Note that the conductor on the north end of the NAB line is essentially coincident with the conductive layer on east end of the A-profile (Figure 13). While the exact resistivity and the location of the deeper conductors on the A-profile may be influenced by 3-D effects, there is reasonable agreement between the two models. Both the A-profile and NAB profile indicate an upper mantle conductor beneath the northern edge of the Buffalo Head Hills.

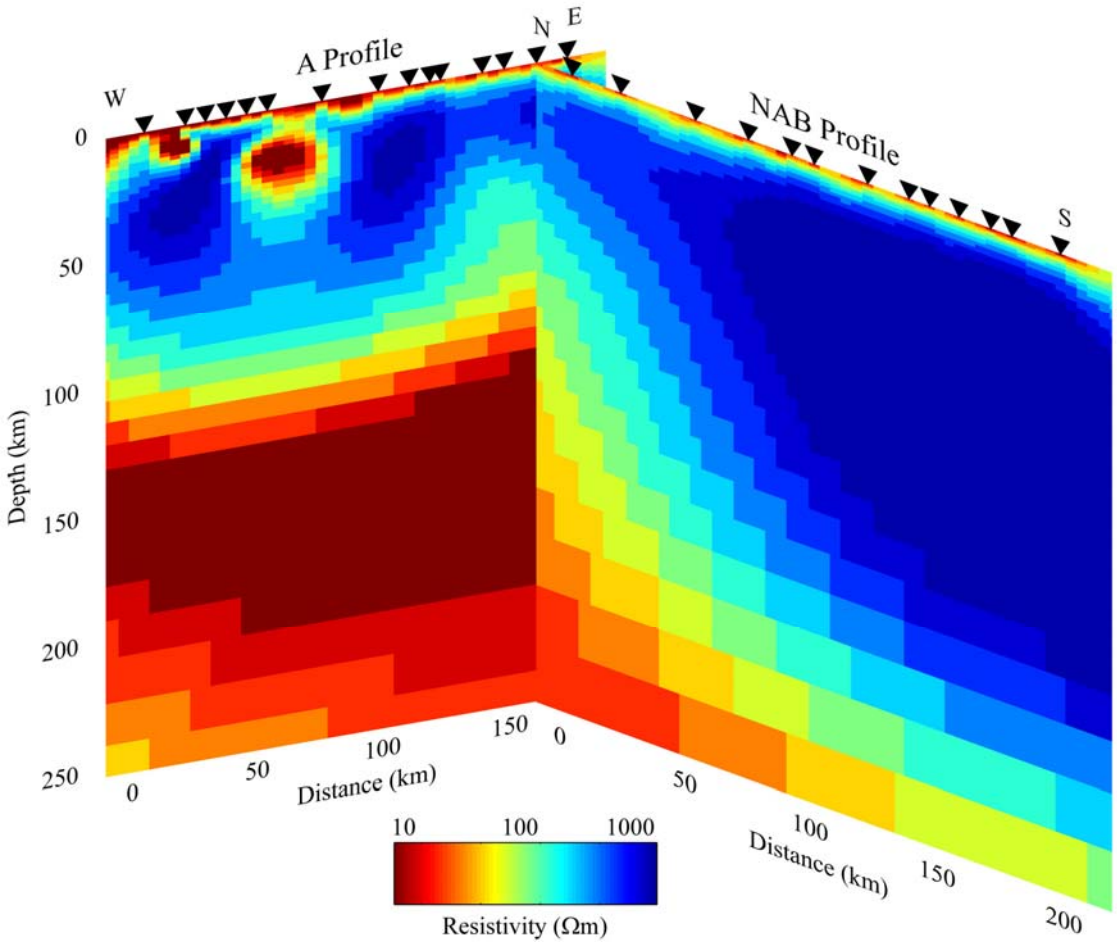

Figure 13. Stitched resistivity models for the NAB profile and LITHOPROBE A-profile (τ =10 and α =3). Low resistivity anomalies on the western half of the A-profile at 20 to 30 km depth are due to the Kiskatinaw conductor (Boerner et al., 2000).

6.2 Three-Dimensional MT Inversion

The data presented in sections 5.1 and 5.2, combined with the mutual consistency of the 2-D inversions, suggest the 2-D inversions are valid and roughly represent the geometry of the conductivity anomaly. However, it is still not precluded that the conductive zone imaged beneath the northern end of Buffalo Head Hills could be the result of a 3-D effect in the MT data incorrectly interpreted by the 2-D inversions.

Before interpreting the resistivity models in detail it is necessary to determine the validity of the 2-D inversion. The most effective way to do this is to undertake 3-D inversion or forward modelling of the data. A 3-D inversion is much more demanding than a 2-D inversion in terms of computer time and memory requirements. The Northern Alberta MT data were inverted using the WSINV3-DMT algorithm of Siripunvaraporn et al., (2005) that was released to academic researchers in February 2006. Computational requirements meant that the number of cells in the vertical and horizontal directions was less in the 3-D inversion than the 2-D inversions previously described and, thus, the 3-D inversion models appear blockier than those derived from 2-D inversions. It should also be noted that spatial distribution of the stations is far from uniform and there are large gaps within the study area where there are no stations. To implement a 3-D inversion it was necessary to reduce the number of stations by selecting one of a group of closely spaced stations. The 3-D inversion used the full impedance tensor with an error floor of

10%. An initial r.m.s misfit of 5.3 was reduced to 0.98 after 6 iterations to yield the model shown in Figure 14. A comparison of Figures 13 and 14 shows that the 3-D inversion model is broadly consistent with the 2-D inversion models. Note that 2-D inversion of the individual profiles was applied after projecting the stations onto a line perpendicular to the strike direction. Therefore, 2-D sections of these profiles are shorter than the actual profile lengths shown on maps and used in the 3-D inversion.

The 3-D model is shown as slices in Figure 15 and the main geoelectric features are as follows

Shallow conductor: This feature is located at 0 to 5 km depth and corresponds to sedimentary rocks of the Western Canada Sedimentary Basin. The 3-D inversion model images variations in thickness of the sedimentary basin along the profiles as seen in Figure 14. Note that the basin is reliably imaged, even with a reduced number of MT stations and reduced number of periods per decade.

Crustal conductors: Firstly, a section view of the 3-D inversion along the A-profile (Figure 14) shows a well-defined crustal conductor on the western half of the profile which corresponds to the previously named Kiskatinaw conductor at a depth of 10 to 30 km. An east section view between B and L reveals two different conductors at different depths (Figure 14). The western conductivity anomaly corresponds to the southern extension of the Kiskatinaw conductor and the eastern anomaly appears as an independent conductor in the south. Just north of the B-profile the two conductors appear to merge. Furthermore, the eastern anomaly shows similar depth extent to the A-profile, whereas the western anomaly extends below the Moho. However, it should also be noted that the resolution decreases in the centre of the study area as the stations' spacing becomes wider.

Upper mantle conductors: An upper mantle conductor is also visible on the eastern half of the A-profile, which appears to coincide with an upper mantle conductor at the northern end of the NAB profile at 50 km depth. As in the 2-D inversions, an upper mantle conductivity anomaly was observed on the northern end of the NAB profile at the joint with A-profile. This anomaly appears to be a well-constrained feature as the final r.m.s fit of the model is ~1 but the spatial data coverage does not allow the extent of this feature to be mapped with confidence (Figure 15).

Asthenosphere: A deep conductor is observed across most of the 3-D resistivity model. This feature is likely the top of the asthenosphere with the lithosphere-asthenosphere boundary at a depth of 200 ± 50 km. Note that the 3-D inversion of the data reveals the LAB to be 200 ± 50 km below even the A, B and L profiles that have shallow conductors, which may alter the deeper resolution of the longer period MT data. The only exception occurs on the western end of the B and L profile due to reduced penetration of electromagnetic waves in the presence of extensive conductivity in this region.

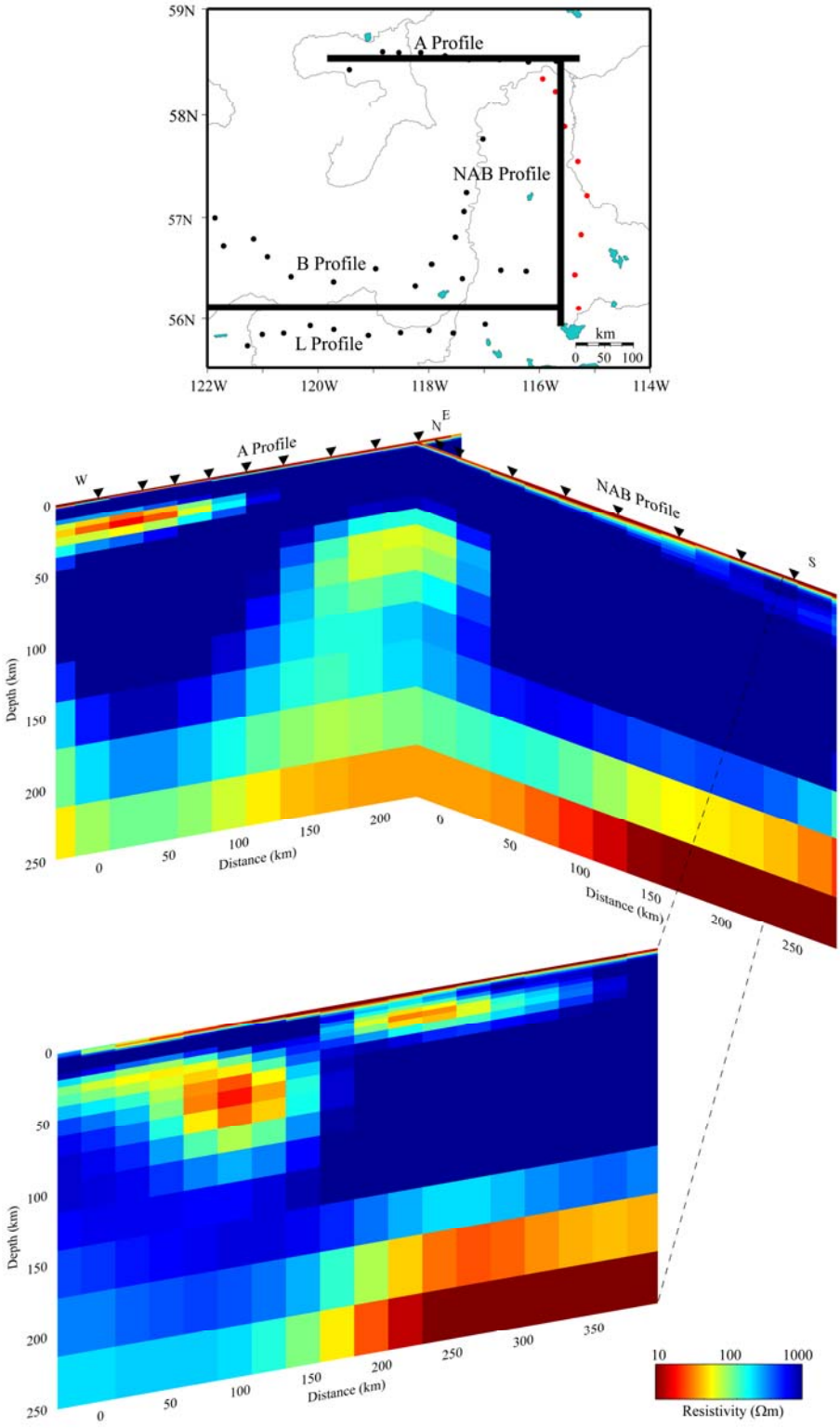

Figure 14. Section views of the 3-D inversion for A-profile, NAB profile and a representative slice between B and L profiles (on the bottom). Dashed lines indicate the true location of the edge of the section as it is offset for a better view.

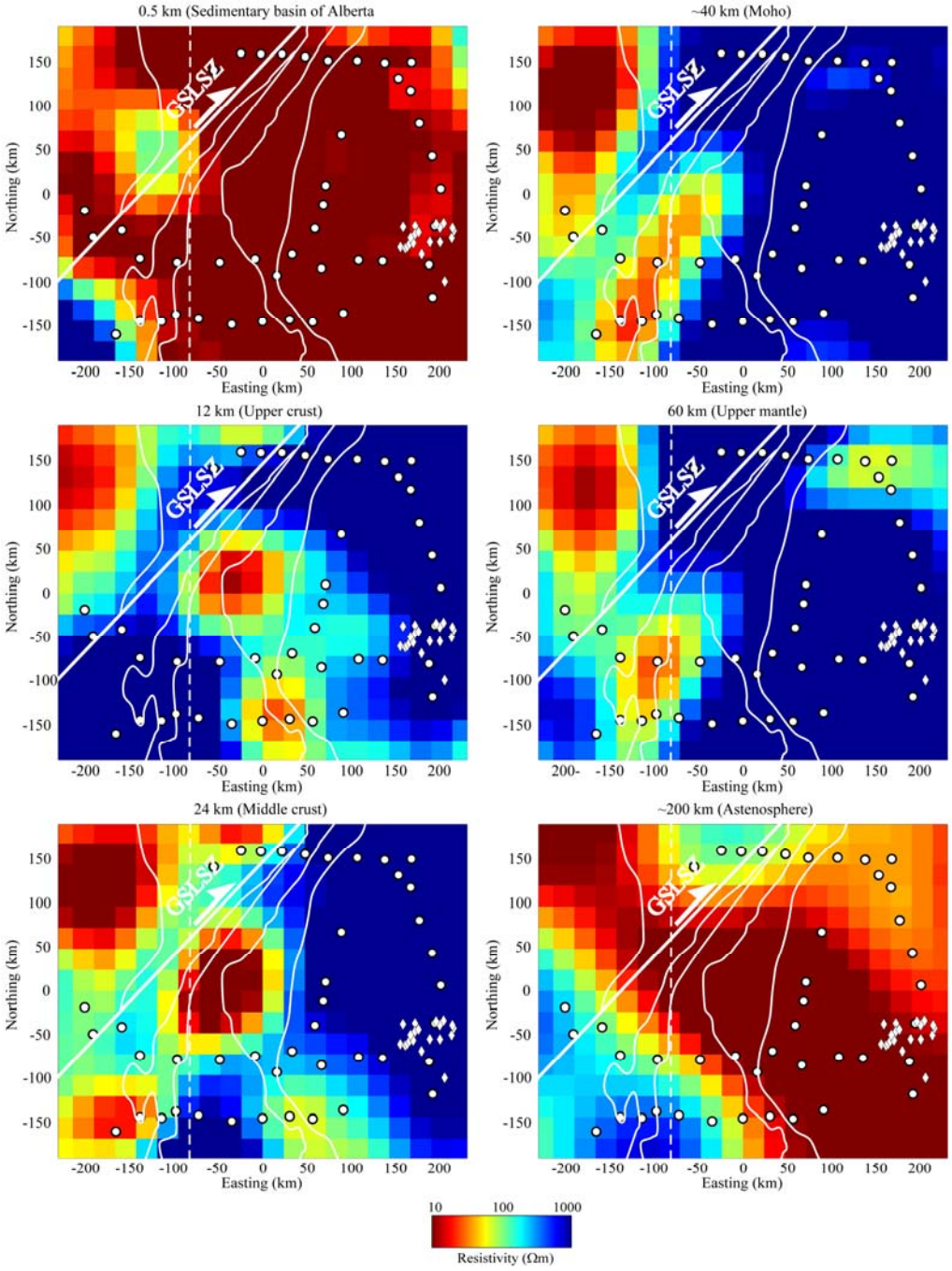

Figure 15. Depth slices of the resistivity model derived by 3-D inversion of the Northern Alberta long-period MT data. White dots show MT stations and diamonds mark kimberlite pipes.

7 Interpretation

The surface layer of low resistivity (10 Ωm) about 5 km thick is well imaged in both the 2-D and 3-D inversion models (Figures 13, 14 and 15). The low resistivity anomaly depicts high-conductivity sedimentary rocks of the Alberta Basin, which contain a significant amount of pore fluids. However, the MT data collected in this study were not intended to give a clear image of the sedimentary basin. This would require a shorter inter station spacing and higher frequency MT data as shown by Xiao and Unsworth (2006). The 3-D inversion provided a better lateral resolution over 2-D inversion, as fewer approximations are made in representing the subsurface resistivity structure. The interstation spacing is also larger than the approximate thickness of the basin, further compromising our ability to image variations of basin depth along the profile.

Beneath the low-resistivity Alberta basin, a high-resistivity (3000 Ωm) thick layer was imaged extending to depths of approximately 200 km. The top of this layer corresponds to the cover/crystalline basement interface. The lower part of this layer consists of lower crustal and upper mantle rocks. This layer is relatively homogenous on the southern half of the NAB profile and an upper mantle conductor is observed at the northern end rising to depths of 50 to 60 km. The characteristics of the NAB profile differ from the LITHOPROBE profiles in the study area. The other three profiles (A, B and L) are affected by large scale, 3-D geoelectric effects that may require anisotropy to explain the MT data (Boerner et al., 2000). These profiles are affected by shallow crustal conductors that, unfortunately, reduce the penetration depth of MT signals. Therefore, resolving the LAB boundary with the LITHOPROBE MT profiles is quite complicated. In contrast, serious 3-D effects are not observed on the NAB data and it is simpler to interpret the depth to lithosphere-asthenosphere boundary. The deeper conductor, which starts at ~200 km, is a robust feature that can be recovered with a range of inversion settings (Figure 12) and is interpreted as the asthenosphere. This boundary corresponds to the LAB and the depth has been verified by 3-D inversion described in the previous section. The LAB depth in this region was defined with teleseismic data at a depth of 200–250 km (Shragge et al., 2002) and, based on petrological/geochemical studies, inferred at a depth of ~180 km (Aulbach et al., 2004). These depths are consistent with the estimates derived from the MT data. The thickness of the lithosphere imaged by MT is approximately constant along the NAB profile, which is not in complete agreement with the suggestion that the lithosphere is thicker beneath the northern half of the Buffalo Head Hills kimberlite field (Hood and McCandless, 2004). However, the diffusive nature of the MT signals means that horizontal variations in LAB depth over distances of <10 km cannot be resolved; therefore, these two datasets may still be compatible. The presence of an upper mantle conductor combined with a deeper (200 km) conductor could be interpreted as a dramatic shallowing of the asthenosphere. However, a combined interpretation of the MT, teleseismic and thermobarometric data is inconsistent with this explanation.

These independent measurements of lithospheric thickness give evidence that the upper mantle conductor beneath the Northern Buffalo Head Hills cannot be due to partial melting. As in the Slave craton, the most plausible explanations are sulphide minerals or graphite films (Jones and Craven, 2004). Xenolith studies in the Slave craton showed no evidence of sulphides, which left graphite as the most viable explanation for the high conductivity in the upper mantle. The presence of sulphides in the upper mantle beneath Northern Alberta has not been documented, and therefore, cannot be excluded as a cause for the low resistivity. Graphite also remains a possible explanation for the low resistivity of the upper mantle, consistent with a depth to the LAB in Northern Alberta of 200 ± 50 km, which lies below the graphite-diamond stability field (~150 km). This can be compared with the value of 260 ± 50 km in Slave craton (Jones and Craven, 2004). Therefore, the depth of LAB in the study area satisfies one of the requirements of diamond-bearing kimberlites. Geochemical studies on kimberlite samples showed that the Buffalo Head Terrane is essentially lherzolitic and the source of the diamonds is predominantly eclogitic and sublithospheric (Hood and McCandless, 2004). Therefore, upper mantle conductivity anomalies just above the graphite-diamond stability field might be due to highly depleted, harzburgitic horizons where

fugacity of oxygen is low enough for carbon to be formed (Thomas Stachel, personal communication, 2005).

In contrast to the Slave craton, the upper mantle conductor in Northern Alberta is not located directly beneath the surface exposure of the kimberlites. This offset is similar to the Saskatchewan mantle conductor that was detected close to the Fort à la Corne kimberlites (Jones et al., 2005). While there are some limitations imposed by the non-uniform MT station coverage, the consistency of the 2-D and 3-D resistivity models gives sufficient evidence that there is no upper mantle conductor beneath the Buffalo Head Hills kimberlite field as currently defined. This suggests that a simple spatial correlation, as observed in the Slave craton, is not a universal phenomenon. However, additional MT data collection is needed to understand reliably other factors that may have changed the resistivity of the lithosphere over time and to validate the 2-D data analysis used in this, and other lithospheric MT studies.

8 Conclusions

In this study, a preliminary 3-D resistivity model has been derived for the Buffalo Head Hills kimberlite province using long-period MT data. The main objective of the study was to assess the validity of previously inferred relationships between diamondiferous kimberlite fields and underlying zones of low resistivity in the lithospheric mantle. This shows that an enhanced upper-mantle conductivity zone is present beneath the northern end of the Buffalo Head Hills but does not exactly underlie the kimberlites. More densely spaced MT stations in the middle and around the northwest corner of the study area are required to map the crustal and upper mantle anomalies and validate the 2-D data analysis approach.

9 References

Ashton Mining of Canada Inc. (1998): Ashton reports analysis and progress of field programs; news release transmitted by Canadian Corporate News. July 27, 1998.

Ashton Mining of Canada Inc. (1999): Ashton reports diamond analysis for kimberlite K11; News release transmitted by Canadian Corporate News. January 15, 1999.

Ashton Mining of Canada Inc. (2001): K252 mini-bulk sample returns 55.0 cpht; News release transmitted by Canadian Corporate News, May 24, 2001.

Ashton Mining of Canada Inc. (2001): Ashton Mining of Canada 2002 Annual Report; <http://www.ashton.ca/news/newsrelease.html>.

Atkinson, E. and Pryde, R. (2006): Seismic investigation of selected kimberlite pipes in the Buffalo Head Hills kimberlite field, north-central Alberta; Alberta Energy and Utilities Board, EUB/AGS Special Report 079, poster.

Aulbach, A., Griffin, W.L., O'Reilly, S.Y. and McCandless, T.E. (2004): Genesis and evolution of the lithospheric mantle beneath the Buffalo Head Terrane, Alberta (Canada); Lithos, v. 77, p. 413-451.

Bahr, K. (1988): Interpretation of the magnetotelluric impedance tensor: regional induction and local telluric distortion; Journal of Geophysics, v. 62, p. 119–127.

Boerner, D.E., Kurtz, R.D., Craven, J.A., Ross, G.M., Jones, F.W. and Davis W.J. (1999): Electrical conductivity in the Precambrian lithosphere of Western Canada; Science, v. 283, p. 668–670.

Boerner, D.E., Kurtz, R.D., Craven, J.A., Ross, G.M. and Jones, F.W. (2000): A synthesis of EM studies in the LITHOPROBE Alberta Basement Transect: constraints on Paleoproterozoic indentation tectonics; Canadian Journal of Earth Sciences, v. 37, p. 1509-1534.

Boyd, F.R. and Gurney, J.J. (1986): Diamonds and the African lithosphere; Science, v. 232, p. 472-477.

Burwash, R.A., Krupicka, J. and Wijbrans, I.R. (2000): Metamorphic evolution of the Precambrian basement of Alberta; Canadian Mineralogist, v. 38, p. 423-434.

Cagniard, L. (1953): Basic theory of the magnetotelluric method of geophysical prospecting; Geophysics, v. 18, p. 605-635.

Cant, D. J. (1988): Regional structure and development of the Peace River Arch, Alberta: a Paleozoic failed rift system?; Bulletin of Canadian Petroleum Geology, v. 36, p. 284-295.

Carlson, S.M., Hillier, W.D., Hood, C.T., Pryde, R.P. and Skelton, D.N. (1998): The Buffalo Hills kimberlite province, north-central Alberta, Canada; *in* Seventh International Kimberlite Conference, Cape Town, Extended Abstracts, p. 138-140.

Clifford, T.N. (1966): Tectono-magmatic-units, metallogenic provinces of Africa; Earth Planet Science Letters, v. 1, p. 421–434.

Chacko, T. De, K.S., Creaser, R.A. and Muehlenbachs, K. (2000): Tectonic setting of the Taltson magmatic zone at 1.9-2.0 Ga: a granitoid-based perspective; Canadian Journal of Earth Science, v. 37, p. 1597-1609.

Chen, D. and Olson, R. (2005): Regional stratigraphic framework of Buffalo Head Hills–Peerless Lake region, northern Alberta; Alberta Energy and Utilities Board, EUB/AGS Earth Sciences Report 2005-05, 40 p.

Davies, R.M., Griffin, W.L., O'Reilly, S.Y. and McCandless, T.E. (2004): Inclusions in diamonds from the K14 and K10 kimberlites, Buffalo Hills, Alberta, Canada: diamond growth in a plume?; Lithos, v. 77, p. 99-111.

De, K. S., Chacko, T., Creaser, R.A. and Muehlenbachs, K. (2000): Geochemical and Nd-Pb-O isotope systematics of granites from the Taltson Magmatic Zone, northeast Alberta: implications for early Proterozoic tectonics in western Laurentia; Precambrian Research, v. 102, p. 221-249.

Eccles, D.R., Heaman, L. M., Luth, R. W. and Creaser, R. A. (2004): Petrogenesis of the northern Alberta kimberlite province; Lithos, v. 76, iss. 1-4 [SPECIAL ISSUE], p. 435-459.

Eccles, D.R., Payne, J.G., Simonetti, A. and Hood, C.T.S. (2006): Petrography and geochronology of crustal xenoliths from northern Alberta kimberlite; Alberta Energy and Utilities Board, EUB/AGS Geo-Note 2006-01, 24 p.

Fulton, R.J. (1989): Foreword to the Quaternary geology of Canada and Greenland; *in* Quaternary Geology of Canada and Greenland, R.J. Fulton (ed.), Geological Survey of Canada, Geology of Canada No. 1 (also Geological Society of America, The Geology of North America, v. K-1), p. 1-11.

Gamble, T.D., Goubau, W.M. and Clarke J. (1979): Magnetotellurics with a remote reference; Geophysics, v. 44, p. 53-68.

Hamilton, W.H., Langenberg, W., Price, M.C. and Chao, D.K. (1999): Geological map of Alberta; Alberta Energy and Utilities Board, EUB/AGS Map 236, scale 1:1 000 000.

Heise, W. and Pous, J. (2001): Effects of anisotropy on the two-dimensional inversion procedure; Geophysical Journal International, v. 147, p. 610-621.

Hood, C.T.S. and McCandless, T.E. (2004): Systematic variations in xenocryst mineral composition at the province scale, Buffalo Hills kimberlites, Alberta, Canada; Lithos, v. 77, p. 733-747.

Jones, A.G. and Craven, J.A. (2004): Area selection for diamond exploration using deep probing electromagnetic surveying; Lithos, v. 77, p. 765-782.

Jones, A.G., Ledo, J. and Ferguson, I. (2005): Electromagnetic images of the Trans-Hudson Oregon: the North American Central Plains anomaly revealed; Canadian Journal of Earth Sciences, v. 42, p. 457-478.

Jones, F.W., Munro, R.A., Craven, J.A., Boerner, D.E., Kurtz, R.D. and Sydora, R.D. (2002): Regional geoelectrical complexity of the Western Canada Basin from magnetotelluric tensor invariants; Earth Planets Space, v. 54, p. 899–905.

Lyatsky, H. and Pană, D. (2003): Catalogue of selected gravity and magnetic maps of northern Alberta; Alberta Energy and Utilities Board, EUB/AGS, Special Report 56, 37 p.

Lyatsky, H., Pană, D., Olson, R. and Godwin, L. (2004): Detection of subtle basement faults with gravity and magnetic data in Alberta Basin, Canada: a data-use tutorial; The Leading Edge, v. 23, p. 1282-1288.

McNeice, G.M. and Jones, A.G. (2001): Multisite, multifrequency tensor decomposition of magnetotelluric data; Geophysics, v. 66, p. 158-173.

O'Connell, S.C., Dix, G.R. and Barclay, J.E. (1990): The origin, history, and regional structural development of the Peace River Arch, Western Canada; Bulletin of Canadian Petroleum Geology, v. 38A, p. 4-24.

Paganelli, F. Grunsky, E.C., Richards, J.P. and Pride, R. (2003): Use of RADARSAT-1 principal component imagery for structural mapping: a case study in the Buffalo Head Hills area, northern central Alberta, Canada; Canadian Journal of Remote Sensing, v. 29, no. 1, p. 111-140.

Pană, D., Waters, E.J. and Grobe, M. (2001): GIS compilation of structural elements in northern Alberta; Alberta Energy and Utilities Board, Earth Sciences Report 2001-01, 32 p.

Parkinson, W.D. (1959): Directions of rapid geomagnetic fluctuations; Geophysical Journal of the Royal Astronomical Society, v. 2, p.1–14.

Partzsch, G.M., Schilling, F.R. and Arndt, J. (2000): The influence of partial melting on the electrical behaviour of crustal rocks: laboratory examinations, model calculations and geological interpretations; Tectonophysics, v. 317, p.189–203.

Paulen, R.C., Fenton, M.M. and Pawlowicz, J.G. (2006): Surficial geology of the Peerless Lake area (NTS 84B); Alberta Energy and Utilities Board, EUB/AGS Map 269, scale 1:250 000.

Pawlowicz, J.G., Prior, G.J., Dolby, G., Eccles, D.R. and Fenton, M.M. (2005a): Early to Late Campanian palynological ages of mudstone and siltstone in the Sawn Lake area, southern Buffalo Head Hills, Alberta; Alberta Energy and Utilities Board, EUB/AGS Geo-Note 2005-01, 43 p.

Pawlowicz, J.G**.,** Fenton, M.M. and Weiss, J. (2005b): Auger core lithologs, Sawn Lake area, southern Buffalo Head Hills, Alberta; Alberta Energy and Utilities Board, EUB/AGS Geo-Note 2005-07, 19 p.

Pilkington, M., Miles, W.F., Ross, G.M. and Roest, W.R. (2000): Potential-field signatures of buried Pre-Cambrian basement in the Western Canada Sedimentary Basin; Canadian Journal of Earth Sciences, v. 37, p. 1453-1471.

Price, R. (1994): Cordilleran tectonics and the evolution of the Western Canada Sedimentary Basin; *in* Geological Atlas of the Western Canada Sedimentary Basin, G.D. Mossop and I. Shetsen (comp.), Canadian Society of Petroleum Geologists and Alberta Research Council, Special Report 4, Chapter 2, p. 13-24.

Rangers, I.M. (2004): Petrology and geochronology from basement core of the Paleoproterozoic Red Earth Granulite Domain, north-central Alberta; M.Sc. thesis, University of Alberta, 175 p.

Rodi, W. and Mackie, R.L. (2001): Nonlinear conjugate gradients algorithm for 2-D magnetotelluric inversion; Geophysics, v. 66, p. 174-187.

Ross, G.M., Parrish, R.R., Villeneuve, M.E. and Bowring, S.A. (1991): Geophysics and geochronology of the crystalline basement of the Alberta Basin, Western Canada; Canadian Journal of Earth Sciences, v. 28, p. 512–522.

Ross, G.M., Mariano, J. and Dumont, R. (1994): Was Eocene magmatism widespread in the subsurface of Southern Alberta? Evidence from new aeromagnetic data; LITHOPROBE Alberta Basement Transect, Report 37, p. 240-249.

Ross, G.M. and Eaton, D. (1999): Basement reactivation in the Alberta Basin: observational constraints and mechanical rationale; Bulletin of Canadian Petroleum Geology, v. 47, p. 391-411.

Ross, G.M. and Eaton, D.W. (2002): Proterozoic tectonic accretion and growth of western Laurentia: results from LITHOPROBE studies in northern Alberta; Canadian Journal of Earth Sciences, v. 39, p. 313-329.

Schilling, F.R., Partzsch, G.M., Brasse, H. and Schwarz, G. (1997): Partial melting below the magmatic arc in the central Andes deduced from geoelectromagnetic field experiments and laboratory data; Physics of the Earth and Planetary Interiors, v. 103, p. 17-31.

Schmucker, U. (1970): Anomalies of geomagnetic variations in the south-western United States; Bulletin Scripps Institute of Oceanography, v. 13, p. 1-165.

Shragge, J., Bostock, M.G., Bank, C.G. and Ellis, R.M. (2002): Integrated teleseismic studies of the southern Alberta upper mantle; Canadian Journal of Earth Sciences, v. 39, p. 399-411.

Skelton, D., Clements, B., McCandless, T.E., Hood, C., Aulbach, S., Davies, R. and Boyer, L.P. (2003): The Buffalo Head Hills kimberlite province, Alberta; *in* Slave Province and Northern Alberta Field Trip Guidebook, B.A. Kjarsgaard (ed.), Guidebook prepared for the 8th International Kimberlite Conference, Victoria, p. 11-20.

Simpson, F. and Bahr, K. (2005): Practical Magnetotellurics; Cambridge University Press, New York, New York, 270 p.

Swift, C.M. (1967): A magnetotelluric investigation of electrical conductivity anomaly in the southwestern United States; Ph.D. thesis, Massachusetts Institute of Technology (reprinted in Vozoff, K. (ed.), 1988, *Magnetotelluric Methods*, Geophysics Reprint Series no. 5, p. 156–166).

Thériault, R.J. and Ross, G.M. (1991): Nd isotopic evidence for crustal recycling in the ca. 2.9 Ga subsurface of western Canada; Canadian Journal of Earth Sciences, v. 28, p. 1140-1147.

Thériault, R.J. (1992): Nd isotopic evolution of the Taltson magmatic zone, Northwest Territories, Canada: insight into Early Proterozoic accretion along the western margin of the Churchill Province; Journal of Geology, v. 100, p. 465-475.

Tikhonov, A.N. (1950): Determination of the electrical characteristics of the deep layers of the Earth's crust; Doklady Akademii Nauk (Proceedings of the Russian Academy of Science), v. 73:2, p. 295-297.

Trommelen, M. (2004): Surficial geology of the Sawn Lake region (84B/13); B.Sc. thesis, University of Alberta, 68 p.

Unsworth, M.J. (2005): New developments in conventional hydrocarbon exploration with EM methods; Canadian Society of Exploration Geophysicist Recorder, April, p. 34-38.

Xiao, W. and Unsworth, M. (2006): Structural imaging in the Rocky Mountain Foothills (Alberta) using magnetotelluric exploration; The American Association of Petroleum Geologists Bulletin, v. 90, no. 3, p. 321-333.

Villeneuve, M.E., Ross, G.M., Parrish, R.R., Theriault, R.J., Miles, W. and Broome, J. (1993): Geophysical subdivision, U–Pb geochronology and Sm–Nd isotope geochemistry of the crystalline basement of the Western Canada sedimentary Basin, Alberta and northeastern British Columbia; Bulletin of Geological Survey of Canada, v. 447, 86 p.

Vozoff, K. (1991): The magnetotelluric method; *in* Electromagnetic Methods in Applied Geophysics, M.N. Nabighian (ed.), Society of Exploration Geophysicists, p. 641-711.

Weaver, J.T., Agarwal, A.K. and Lilley, F.E.M. (2000): Characterization of the magnetotelluric tensor in terms of its invariants; Geophysical Journal International, v. 141, p. 321–336.

Xu, Y., Shankland, T.J. and Poe, B.T. (2000): Laboratory-based electrical conductivity of the Earth's mantle; Journal of Geophysical Research, v. 105, p. 27865–27875.